Viscosity and surface tension of the $Zr_{56.5}Ti_{13.3}Ni_{13.6}Cu_{9.6}S_7$ bulk metallic glass-forming liquid

Lucas Matthias Ruschel ✉ iD ; Alexander Kuball iD ; Bastian Adam iD ; Maximilian Frey iD ; Ralf Busch iD

Check for updates

View Online   Export Citation

Viscosity and surface tension of the $Zr_{56.5}Ti_{13.3}Ni_{13.6}Cu_{9.6}S_7$ bulk metallic glass-forming liquid

Lucas Matthias Ruschel,[1,a] [iD] Alexander Kuball,[2] [iD] Bastian Adam,[1] [iD] Maximilian Frey,[1] [iD] and Ralf Busch[1] [iD]

AFFILIATIONS

[1] Chair of Metallic Materials, Saarland University, 66123 Saarbrücken, Germany
[2] Amorphous Metal Solutions GmbH, 66424 Homburg, Germany

[a] Author to whom correspondence should be addressed: lucas.ruschel@uni-saarland.de

ABSTRACT

The viscosity of the $Zr_{56.5}Ti_{13.3}Ni_{13.6}Cu_{9.6}S_7$ bulk glass forming alloy was measured in equilibrium liquid at low and high temperatures. Low temperature measurements were conducted in the vicinity of the glass transition using a thermomechanical analyzer, covering a viscosity range between 10^9 and 10^{14} Pa s. The high-temperature experiments were carried out by electromagnetic levitation of a spherical droplet in microgravity during a parabolic flight campaign (TEMPUS), ranging in viscosity from 50 to 800 mPa s. The viscosities were individually modeled using the Vogel–Fulcher–Tammann equation to obtain the fragility parameter D^*, which displays a strong liquid behavior of 25.8 and 19.6 for the low and high temperature region, respectively. The Mauro–Yue–Ellison–Gupta–Allan viscosity model was additionally applied, revealing an even more accurate description across the whole temperature range. Next to viscosity, TEMPUS measurements allow the determination of surface tension. With a value of 0.9 N m^{-1}, it is significantly lower than that of other Zr-based metallic glasses without the element sulfur.

I. INTRODUCTION

Zr-based bulk metallic glasses (BMGs) are among the best metallic glass forming systems and are specifically interesting due to their high strength, hardness, low Young's modulus, large elastic limit, and good biocompatibility.[1,2] This specific class is among the first to achieve fully amorphous rods above 1 cm, with $Zr_{41.2}Ti_{13.8}Cu_{12.5}Ni_{10}Be_{22.5}$ (Vit1) as the first commercial BMG.[3,4] Most of the alloys developed in this early development period possess Be as alloying element, which is nowadays unwanted due to its hazardous nature, restricting the usage of these alloys. Therefore, many different Zr-based bulk metallic glasses without the element Be were developed, with the most important being Zr–Cu–Al type derivates. Two widespread alloys belonging to this class are $Zr_{59.3}Cu_{28.8}Al_{10.4}Nb_{1.5}$ (AMZ4) and $Zr_{52.5}Cu_{17.9}Ni_{14.6}Al_{10}Ti_5$ (Vit105), which are both extensively studied in the literature due to their high potential for industrial applications.[5–8]

Alternatively, it has recently been shown that sulfur is highly favorable for glass formation on the Ti-rich side of the Zr–Ti–Cu–Ni system.[9,10] One major advantage of these sulfur-bearing BMGs in comparison to other established bulk glass forming alloys is their resistance against oxygen impurities in terms of glass forming ability (GFA) and mechanical properties. This enables the use of industrial grade material, which substantially decreases the material costs.[11] Alloy development toward higher Zr-contents led to the bulk glass forming composition $Zr_{56.5}Ti_{13.3}Ni_{13.6}Cu_{9.6}S_7$, which turned out to be the best compromise between GFA and size of the supercooled liquid region (SCLR).[11] Thus, this alloy is not only interesting for casting processes but also for processing techniques such as thermoplastic forming[12,13] or the uprising additive manufacturing technique of selective laser melting.[14–16] Especially the latter is currently a "hot topic" in the metallic glass community and is emerging as an important production route for upscaling of amorphous parts.[17] Moreover, this process does not require a large critical casting size

as the powder feedstock material is molten locally with a laser, enabling high cooling rates in the order of 10^4–10^6 K s^{-1}.[6] For processing techniques such as thermoplastic forming, cast as well as printed parts are allowed to be shaped without high forces as the viscosity changes several orders of magnitude in the SCLR.[13,18,19] Therefore, the knowledge of viscosity across a large temperature range is essential for simulation of these processes.

In this study, we measured the viscosity in the deeply SCLR with a thermomechanical analyzer, as well as in the equilibrium liquid at high temperatures by applying the oscillation droplet method in weightlessness during a parabolic flight campaign. In case of $Zr_{56.5}Ti_{13.3}Ni_{13.6}Cu_{9.6}S_7$, the liquid viscosity behavior can be modeled using the Vogel–Fulcher–Tammann (VFT) and Mauro–Yue–Ellison–Gupta–Allan (MYEGA) equation over 16 orders of magnitude, which is unusual as the most systems reported so far, especially Zr-based alloys without sulfur, cannot be fitted with a single equation due to the so called fragile-to-strong transition.[20]

II. EXPERIMENTAL PROCEDURE

A. Sample production and characterization

The $Zr_{56.5}Ti_{13.3}Ni_{13.6}Cu_{9.6}S_7$ master alloy was produced from high purity raw elements Zr (99.99 wt. %), Ti (99.999 wt. %), Cu (99.95 wt. %), Ni (99.95 wt. %), and an inductively custom-made $Ni_{55}S_{45}$ (at. %) pre-alloy (S purity - 99.9995 wt. %) by arc-melting under a Ti-gettered high purity Ar atmosphere. The detailed production process of a similar pre-alloy is described elsewhere.[21] Amorphous specimens were obtained by arc-melting and suction-casting into water-cooled Cu molds. Their glassy structure was verified by x-ray diffraction (XRD) and further characterized by the differential scanning calorimetry (DSC) technique.

B. Low-temperature viscosity

The low temperature viscosity around the glass transition was determined using a Netzsch TMA 402 F3 Hyperion thermomechanical analyzer (TMA) in a three-point beam bending setup. A rectangular beam shaped specimen was loaded centrally with a constant force of 0.1 N, while the deflection rate was measured during the experiment. Two different measurement techniques were applied by measuring in the scan mode with a constant heating rate of 0.33 K s^{-1} and isothermally at different temperatures below T_g. Both protocols resulted in a deflection of the beam with a midpoint deflection rate v, allowing the determination of the temperature-dependent viscosity according to[22]

$$\eta = -\frac{gL^3}{144 I_c v}\left[M + \frac{\rho A L}{1.6}\right], \qquad (1)$$

with g being the gravitational constant, L being the support span, I_c ($= bh^3/12$; b = width and h = thickness) being the moment of inertia of a rectangular beam, M being the loading mass, ρ being the density of the composition, and A being the cross-sectional area.

In case of an isothermal heating protocol, the relaxation of viscosity into the equilibrium liquid can be described using the Kohlrausch–Williams–Watts (KWW) equation,[23]

$$\eta(t) = \eta_g + \eta_{eq-g}\left[1 - \exp\left(-\left(\frac{t}{\tau}\right)\right)\right], \qquad (2)$$

with $\eta(t)$ being the viscosity, η_g being the initial viscosity of the glass before relaxation, η_{eq-g} being the viscosity increase during relaxation into the equilibrium liquid, t being the time, τ being the relaxation time, and β being the stretching exponent. The viscosity of the equilibrium liquid is determined as $\eta_{eq} = \eta_g + \eta_{eq-g}$.

C. High-temperature viscosity and surface tension

Container-less electromagnetic levitation of a metallic droplet in microgravity (TEMPUS) is an ideal method to determine the high temperature viscosity and surface tension of highly reactive Zr melts.[24–26] TEMPUS provides comparable viscosity and fragility results to common methods such as Couette viscometry or electrostatic levitation, with the advantage that no crucible contamination or gravitational forces affect the droplet.[27] A spherical sample (6.5 mm in diameter) was electromagnetically levitated and heated
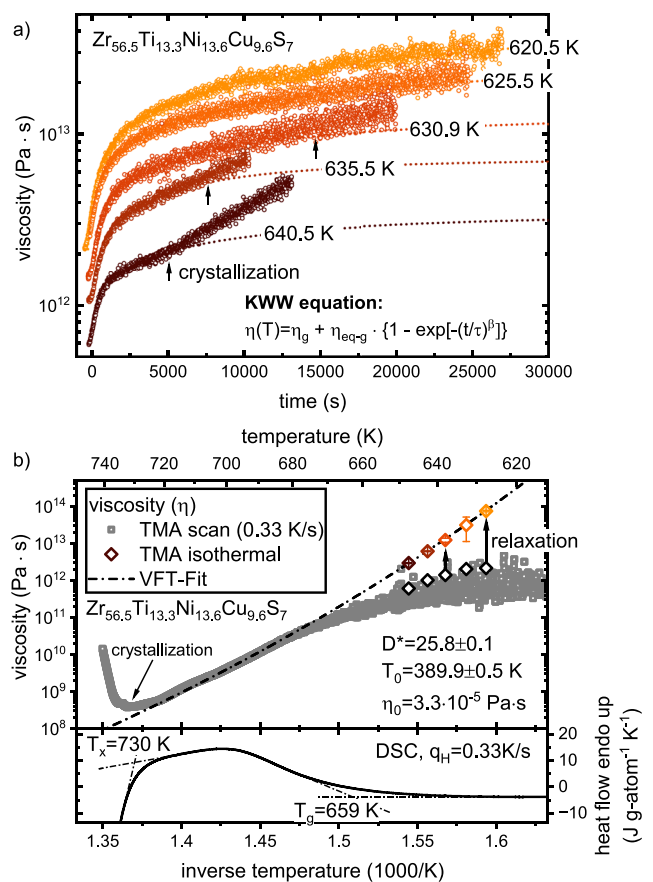
FIG. 1. (a) Isothermal viscosity measurements below the glass transition of $Zr_{56.5}Ti_{13.3}Ni_{13.6}Cu_{9.6}S_7$. The dotted curves represent the KWW fits, which describe the relaxation of the glassy state to the equilibrium liquid state at different temperatures. (b) The equilibrium viscosities are plotted along a TMA scan measurement as a function of inverse temperature. The black dashed line represents the VFT fit, revealing a strong liquid behavior with a D^* of 25.8. The lower panel depicts a DSC scan measured with the same scan rate of 0.33 K s^{-1} for orientation.

up to a maximum of 1900 K during the microgravity phase. During free cooling, the droplet was compressed after a short excitation pulse, resulting in an oscillation decay behavior. The whole process was recorded using a 200 Hz camera, and the movie was further processed using digital image software to obtain the radius change in the droplet in the X- and Y-direction as a function of time. The radius of the droplet as a function of time, $r(t)$, can be described by a damped cosine function,[25]

$$r(t) = r_0 + A \cos(\omega t) \exp(-\Gamma t), \quad (3)$$

with r_0 being the quiescent radius of the sample, A being the amplitude of the oscillation, ω being the angular frequency, and Γ being the damping constant.

The damping constant can then be used, with the knowledge of the sample mass m, to calculate the viscosity of the liquid, according to[28]

$$\eta(T) = \frac{3m\Gamma}{20r_0\pi}. \quad (4)$$

Besides viscosity information, surface tension can be determined from TEMPUS experiments by performing a fast Fourier transform analysis of the damped oscillation to determine the resonant frequency ω_R (more details in the supplementary material and in Fig. SI3).[24] With the known sample mass m, the surface tension γ can be calculated using

$$\gamma = \frac{3}{8}\pi m \omega_R^2. \quad (5)$$

Further details about the oscillation droplet method in microgravity can be found in Refs. 24–26, 28, and 29.

D. Modeling of viscosity

The viscosities in the liquid can be described by different models. Here, the empirical Vogel–Fulcher–Tammann (VFT) relation is used,[30]

$$\eta(T) = \eta_0 \exp\left(\frac{D^* T_0}{T - T_0}\right), \quad (6)$$

with D^* being the fragility parameter, T_0 being the VFT temperature, and η_0 being the pre-exponential factor. At infinitely high temperatures, the viscosity approaches η_0, which can be estimated according to the relation $\eta_0 = N_A \cdot h/V_m$, with N_A being Avogadro's constant, h being Planck's constant, and V_m being the molar volume.[31] For $Zr_{56.5}Ti_{13.3}Ni_{13.6}Cu_{9.6}S_7$, η_0 was calculated to be $\eta_0 = 3.3 \cdot 10^{-5}$ Pa s and used for the fitting.

In addition, the MYEGA (Mauro, Yue, Ellison, Gupta, and Allan) relation, which enables an improved extrapolation of viscosity, can be described as

$$\eta(T) = \eta_0 \exp\left[\ln(10)\frac{B}{T}\exp\left(\frac{C}{T}\right)\right], \quad (7)$$

with η_0 being the pre-exponential factor and B and C being the fitting parameters. More information on the physical background of this equation can be found in Ref. 32.

III. RESULTS

Figure 1(a) shows the viscosity calculated from the TMA deflection experiments for different isothermal temperatures. The viscosity (open circles) is increasing at each temperature during relaxation from the initial glassy state to the supercooled liquid state. The relaxation curves are fitted with the stretched exponential KWW equation (dashed line) to determine the equilibrium viscosity at the given
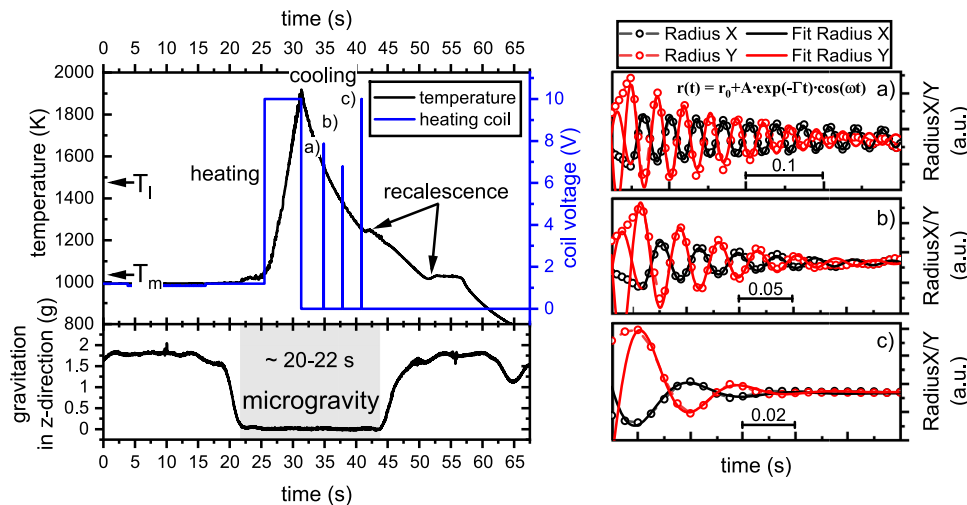
FIG. 2. Temperature, coil voltage, and gravitation as a function of time of one parabola. The spikes in the coil voltage indicate the excitation pulses for the droplet and are labeled (a), (b), and (c). The resulting damped oscillations for the respective pulses are shown in panels (a)–(c) together with the fit of a damped cosine function (Multimedia available online).
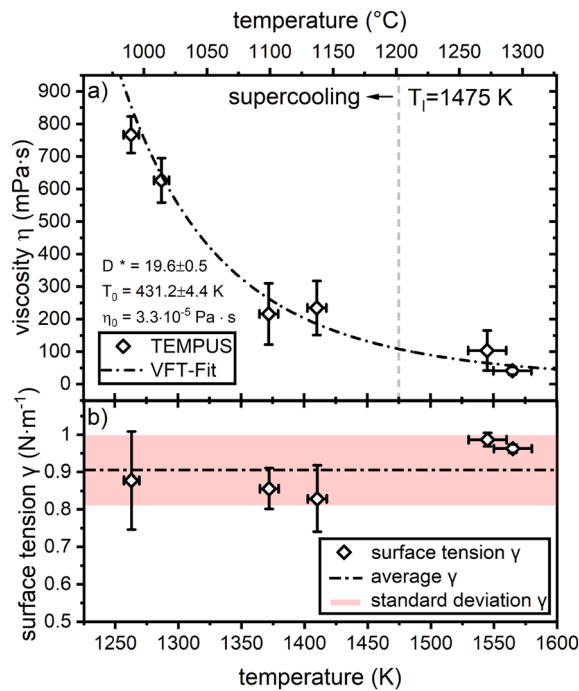
FIG. 3. (a) High-temperature viscosity and (b) surface tension as a function of temperature of $Zr_{56.5}Ti_{13.3}Ni_{13.6}Cu_{9.6}S_7$. For a metallic liquid near T_l, the temperature dependence of viscosity is exceptionally strong, with a fragility parameter D^* of 19.6. The average surface tension is determined to be ~0.9 N m^{-1}, which is rather low compared to that of sulfur-free Zr-liquids.

temperature. The sudden deviation of the viscosity from the fit corresponds to crystallization of the sample, so the equilibrium viscosity at temperatures close to T_g can only be determined via extrapolation. To determine the temperature dependence of viscosity by means of the VFT model, the equilibrium viscosity values are plotted as a function of inverse temperature, as can be seen in Fig. 1(b). The fit yields a fragility parameter D^* of 25.8 and a VFT temperature T_0 of 389.9 K and aligns well with the TMA scan measurement of 0.33 K s^{-1}, which allows the measurement of viscosity in the supercooled liquid prior to crystallization.

Figure 2 shows different important processing parameters of the parabolic flight experiments, such as temperature, coil voltage, and gravitation. Upon starting of the parabola, the gravitational force reaches zero and the sample is heated inductively well above its liquidus temperature, $T_l = 1475$ K. Subsequently, the sample is freely cooled by turning off the heating coil. During cooling, three excitation pulses were applied, which can be seen from the three spikes, labeled (a), (b), and (c), in the coil voltage. The corresponding droplet oscillation for the three pulses in the X- and Y-direction is recorded with a 200 Hz high frequency camera, the analysis of which is shown in the corresponding panels in Fig. 2 (Multimedia view). By increasing cooling from (a) to (c), the oscillation undergoes progressively stronger damping due to the increase in viscosity.

The determined equilibrium viscosities at each temperature shown in Fig. 3(a) correspond to the mean value of the cosine

damped function in the X- and Y-direction. The uncertainty in viscosity corresponds to one standard deviation. The temperature error results from the continuous cooling nature of the experiment, the determination of which is provided in the supplementary material. The viscosity calculated above the liquidus temperature (gray dashed line) is in the region of 100 mPa s, while supercooling below T_l leads to an increase in the range of 250–800 mPa s. The high melt viscosity for the last oscillation might be connected to crystallization as it is close to the first recalescence (see Fig. 2). However, this can be excluded as the last oscillation exhibits a decay time of just 60 ms and is finished before the recalescence sets in. This was double checked using the high frequency camera, where the precipitates are first visible after the last oscillation is finished (see supplementary material video Nr. 1). The high temperature viscosity is also fitted using the VFT-type equation, with the fit pinned to the viscosity at the kinetic glass transition temperature T_g^*, which is 10^{12} Pa s by definition. This results in a relatively strong kinetic fragility behavior with a D^* of 19.6, not far away from the value for the low temperature data. Figure 3(b) shows the calculated surface tension γ at different temperatures. It turns out that the surface tension is almost identical across the measurement range of 300 K (1250–1550 K), which is on average calculated to be 0.9 N m^{-1}.

IV. DISCUSSION

Upon direct comparison of the melt viscosity at the liquidus temperature, $Zr_{56.5}Ti_{13.3}Ni_{13.6}Cu_{9.6}S_7$ possesses a viscosity of around 100 mPa s (see Fig. 3), which is about twice as high as that for Zr-based alloys, such as Vit105 and AMZ4.[20,27] A similar increase in melt viscosity by an addition of S of up to 8 at. % was also observed in the Ti–Ni–S system,[33] which was suspected to be related to higher packing density in the melt as S is a small atomic
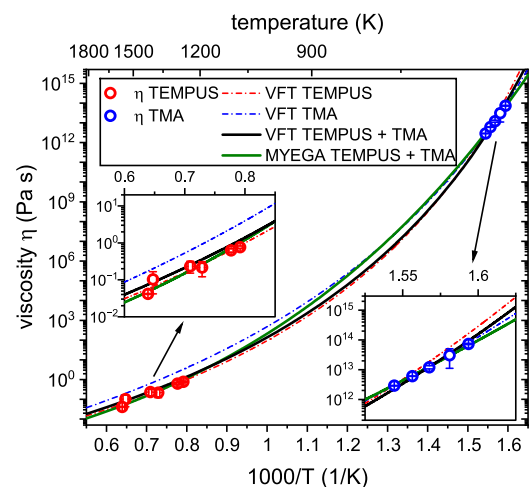
FIG. 4. Viscosity as a function of inverse temperature of $Zr_{56.5}Ti_{13.3}Ni_{13.6}Cu_{9.6}S_7$. The blue and red open circles correspond to the low and high temperature viscosity, respectively. The individual VFT fits are indicated as dashed lines. The combined fits (VFT and MYEGA) are given as solid lines. As can be seen from the two insets, the green solid line gives the best description of viscosity over the whole temperature range.

TABLE I. Fitting parameters to model the viscosity of $Zr_{56.5}Ti_{13.3}Ni_{13.6}Cu_{9.6}S_7$ with the VFT and MYEGA fitting function. The m-fragility is calculated from the fitting parameters of the respective model.

Fit	η_0 (10−5 Pa s)	D^*	T_0 (K)	T_g^* (K)	B (K)	C (K)	m
VFT TMA	3.3	25.8 ± 0.1	389.9 ± 0.5	655	⋯	⋯	40.7
VFT TEMPUS	3.3	19.6 ± 0.5	431.2 ± 4.4	654	⋯	⋯	48.4
VFT TEMPUS+TMA	3.3	21.1 ± 0.5	419.3 ± 2.7	653	⋯	⋯	45.9
MYEGA TEMPUS+TMA	3.3	⋯	⋯	656	2820.0 ± 65.2	880.8 ± 15.0	38.6

species,[34] satisfying the empirical rules for glass formation.[35] However, Wilden *et al.* have shown for the $Ti_{75}Ni_{17}S_8$ alloy that the packing fraction is actually reduced by S addition, which contradicts the experienced increase in viscosity.[33] They interpreted this increase in viscosity to the formation of covalent interaction of S with the constituent atoms, which presumably also applies to the studied alloy of this work, which has a comparable S content. Apart from the increased melt viscosity, the temperature dependence, e.g., fragility, also changes compared to the metalloid-free Zr-alloys mentioned above. Figure 4 combines the viscosity data from both measurement methods in an inverse temperature plot. Different VFT fits are shown, where the high and low temperature data are fitted individually (dashed lines) and together (solid black line). The individual fitted data indicate just a small offset in their temperature dependence of viscosity, although the high temperature liquid behaves in a more fragile manner [D^* (high T) = 19.6 vs D^* (low T) = 25.8]. The observed difference between the high temperature fragile liquid and a low temperature strong liquid is in line with several metallic glass-forming liquids and is associated with a pronounced structural ordering during cooling.[20,27,36–39] A fragile liquid at high temperatures is connected to a less pronounced medium range order, where the temperature dependence of viscosity follows a non-Arrhenius behavior. The deviation from such a non-Arrhenius behavior toward a 'quasi-Arrhenius' behavior (fragile-to-strong transition) is attributed to the formation of densely packed structures, clustering together to form a more pronounced medium range order.[20,40] This implies that the liquid structure must change severely to achieve the sudden increase in viscosity due to the different fragilities.[27,35] For a number of common Zr-based alloys, the fragility switches from about D^* of 10 at high temperature to about D^* of 25 at low temperature.[20,31] This appears to be different or at least less pronounced for the $Zr_{56.5}Ti_{13.3}Ni_{13.6}Cu_{9.6}S_7$ melt as the offset in viscosity is rather small across the studied temperature range, as shown in Fig. 4. This indicates a pronounced medium range order structure already near the liquidus temperature. Therefore, the structural ordering upon supercooling is supposed to be much less pronounced as the difference between high- and low-temperature dependence of viscosity is small. This could possibly be connected to the unique melt structure, brought in by directional bonds with S.[33] However, fitting with a single VFT (D^* = 21.1, T_0 = 419.3 K) or MYEGA equation indicates that such a fragile-to-strong transition might not happen at all as both functions are able to describe the viscosity over 16 orders of magnitude very well. However, the MYEGA fit is ahead as it describes the course of both temperature regions even more accurately with a higher R^2 value of 0.99 compared to the VFT fit with an R^2 value of 0.96. This can also be seen

visually in the insets in Fig. 4. It also avoids the divergence of the VFT fit at T_0, which is an ongoing issue with the lack of experimental evidence of the VFT equation.[41] All fitting parameters as well as the kinetic glass transition temperature T_g^* are summarized in Table I. T_g^* differs slightly depending on the fit, but all agree very well with the measured calorimetric glass transition of 659 K [see Fig. 1(b)]. In addition, the m-fragility was calculated, resembling the steepness and thus the fragility of each fit at T_g^*. The higher the m-value, the steeper the slope, indicating a kinetically more fragile behavior, and vice versa. The most appropriate value for the m-fragility is obtained by the VFT (TMA) and MYEGA fit as they describe the low-temperature region around T_g^* the best. Therefore, the two values (40.7 and 38.6) are very similar and fall within the typical range for bulk metallic glass.[42]

Next to viscosity, the surface tension γ was determined on average to be 0.9 N m^{-1}. This value is nearly identical to the quaternary S-containing alloy on the Ti-rich side $Ti_{60}Zr_{15}Cu_{17}S_8$.[14] This is particularly interesting as the surface tension of metalloid-free Zr-based systems is much higher at around 1.6 N m^{-1} for the alloy AMZ4, which is reduced to 1.4 N m^{-1} using industrial grade material (i.e., higher oxygen contamination). The effect of oxygen and sulfur on the surface tension was already shown in 1982 by Keene *et al.*, where 0.2 wt. % of oxygen and sulfur led to a decrease from 1.8 to 1.2 N m^{-1} in pure iron.[43] Their similar effect on surface tension is likely related to the chemical resemblance of the two elements as they are located next to each other in the same main group of the Periodic Table. Thus, it is not surprising that S also reduces the surface tension in the liquid of Zr-based BMGs as it is used as an alloying element in large quantities. The possibility to tailor the surface tension is generally beneficial as a targeted reduction and can improve the flow of the molten metal during the casting process, resulting in improved filling of cavities.

V. CONCLUSION

To conclude, the bulk metallic glass forming alloy $Zr_{56.5}Ti_{13.3}Ni_{13.6}Cu_{9.6}S_7$ was characterized with respect to its low- and high-temperature viscosity as well as its surface tension in the vicinity of the liquidus temperature:

- The liquid behaves kinetically strong across the entire temperature range and can be modeled with a single VFT equation, whereas the MYEGA fit is even more accurate and thus a better suited viscosity model for this alloy.
- Sulfur reduces the surface tension in the liquid state significantly to 0.9 N m^{-1}, in comparison to S-free Zr-based BMGs possessing a value around 1.6 N m^{-1}.

- In summary, sulfur increases the viscosity of the melt, which is beneficial for glass formation but detrimental for castability. The latter, in turn, can be compensated by the reduced surface tension.

SUPPLEMENTARY MATERIAL

See the supplementary material for the high temperature melting and crystallization calorimetry curve. Additional details on the evaluation of the TEMPUS dataset are provided, in particular the temperature error calculation and the detailed analysis of the surface tension.

AUTHOR DECLARATIONS

Conflict of Interest

The authors have no conflicts to disclose.

Author Contributions

L. M. Ruschel: Conceptualization (equal); Data curation (equal); Formal analysis (equal); Investigation (equal); Methodology (equal); Supervision (equal); Validation (equal); Visualization (equal); Writing – original draft (equal); Writing – review & editing (equal). **A. Kuball**: Data curation (equal); Formal analysis (equal); Funding acquisition (equal); Investigation (equal); Methodology (equal); Project administration (equal); Supervision (equal); Writing – review & editing (equal). **B. Adam**: Formal analysis (equal); Project administration (equal); Validation (equal); Writing – review & editing (equal). **M. Frey**: Project administration (equal); Writing – review & editing (equal). **R. Busch**: Funding acquisition (equal); Project administration (equal); Supervision (equal); Writing – review & editing (equal).

DATA AVAILABILITY

The data that support the findings of this study are available from the corresponding author upon reasonable request.

REFERENCES

[1] A. L. Greer and E. Ma, "Bulk metallic glasses: At the cutting edge of metals research," MRS Bull. **32**, 611–619 (2007).

[2] C. Qiu, Q. Chen, L. Liu, K. Chan, J. Zhou, P. Chen, and S. Zhang, "A novel Ni-free Zr-based bulk metallic glass with enhanced plasticity and good biocompatibility," Scr. Mater. **55**, 605–608 (2006).

[3] A. Peker and W. L. Johnson, "A highly processable metallic glass: $Zr_{41.2}Ti_{13.8}Cu_{12.5}Ni_{10.0}Be_{22.5}$," Appl. Phys. Lett. **63**, 2342–2344 (1993).

[4] W. L. Johnson, "Bulk glass-forming metallic alloys: Science and technology," MRS Bull. **24**, 42–56 (1999).

[5] J. Heinrich, R. Busch, and B. Nonnenmacher, "Processing of a bulk metallic glass forming alloy based on industrial grade Zr," Intermetallics **25**, 1–4 (2012).

[6] J. J. Marattukalam, V. Pacheco, D. Karlsson, L. Riekehr, J. Lindwall, F. Forsberg, U. Jansson, M. Sahlberg, and B. Hjörvarsson, "Development of process parameters for selective laser melting of a Zr-based bulk metallic glass," Addit. Manuf. **33**, 101124 (2020).

[7] R. Al-Mukadam, I. Götz, M. Stolpe, and J. Deubener, "Viscosity of metallic glass-forming liquids based on Zr by fast-scanning calorimetry," Acta Mater. **221**, 117370 (2021).

[8] M. Morrison, R. Buchanan, P. Liaw, B. Green, G. Wang, C. Liu, and J. Horton, "Four-point-bending-fatigue behavior of the Zr-based Vitreloy 105 bulk metallic glass," Mater. Sci. Eng.: A **467**, 190–197 (2007).

[9] A. Kuball, O. Gross, B. Bochtler, and R. Busch, "Sulfur-bearing metallic glasses: A new family of bulk glass-forming alloys," Scr. Mater. **146**, 73–76 (2018).

[10] L. M. Ruschel, B. Adam, O. Gross, N. Neuber, M. Frey, H.-J. Wachter, and R. Busch, "Development and optimization of novel sulfur-containing Ti-based bulk metallic glasses and the correlation between primarily crystallizing phases, thermal stability and mechanical properties," J. Alloys Compd. **960**, 170614 (2023).

[11] A. Kuball, O. Gross, B. Bochtler, B. Adam, L. Ruschel, M. Zamanzade, and R. Busch, "Development and characterization of titanium-based bulk metallic glasses," J. Alloys Compd. **790**, 337–346 (2019).

[12] B. Bochtler, M. Stolpe, B. Reiplinger, and R. Busch, "Consolidation of amorphous powder by thermoplastic forming and subsequent mechanical testing," Mater. Des. **140**, 188–195 (2018).

[13] J. Schroers, "Processing of bulk metallic glass," Adv. Mater. **22**, 1566–1597 (2010).

[14] A. Kuball, "Development, characterization and processing of a novel family of bulk metallic glasses: Sulfur-containing bulk metallic glasses," Ph.D. dissertation (Saarland University, 2019).

[15] H. Y. Jung, S. J. Choi, K. G. Prashanth, M. Stoica, S. Scudino, S. Yi, U. Kühn, D. H. Kim, K. B. Kim, and J. Eckert, "Fabrication of Fe-based bulk metallic glass by selective laser melting: A parameter study," Mater. Des. **86**, 703–708 (2015).

[16] Y. Shen, Y. Li, C. Chen, and H.-L. Tsai, "3D printing of large, complex metallic glass structures," Mater. Des. **117**, 213–222 (2017).

[17] M. M. Khan, A. Nemati, Z. U. Rahman, U. H. Shah, H. Asgar, and W. Haider, "Recent advancements in bulk metallic glasses and their applications: A review," Crit. Rev. Solid State Mater. Sci. **43**, 233–268 (2018).

[18] M. Frey, J. Wegner, N. Neuber, B. Reiplinger, B. Bochtler, B. Adam, L. Ruschel, S. S. Riegler, H.-R. Jiang, S. Kleszczynski, G. Witt, and R. Busch, "Thermoplastic forming of additively manufactured Zr-based bulk metallic glass: A processing route for surface finishing of complex structures," Mater. Des. **198**, 109368 (2021).

[19] Z. Li, Z. Huang, F. Sun, X. Li, and J. Ma, "Forming of metallic glasses: Mechanisms and processes," Mater. Today Adv. **7**, 100077 (2020).

[20] Z. Evenson, T. Schmitt, M. Nicola, I. Gallino, and R. Busch, "High temperature melt viscosity and fragile to strong transition in Zr–Cu–Ni–Al–Nb(Ti) and $Cu_{47}Ti_{34}Zr_{11}Ni_8$ bulk metallic glasses," Acta Mater. **60**, 4712–4719 (2012).

[21] A. Kuball, B. Bochtler, O. Gross, V. Pacheco, M. Stolpe, S. Hechler, and R. Busch, "On the bulk glass formation in the ternary Pd-Ni-S system," Acta Mater. **158**, 13–22 (2018).

[22] H. E. Hagy, "Experimental evaluation of beam-bending method of determining glass viscosities in the range 10^8 to 10^{15} poises," J. Am. Ceram. Soc. **46**, 93–97 (1963).

[23] J. C. Phillips, "Stretched exponential relaxation in molecular and electronic glasses," Rep. Prog. Phys. **59**, 1133–1207 (1996).

[24] I. Egry, "Surface tension measurements of liquid metals by the oscillating drop technique," J. Mater. Sci. **26**, 2997–3003 (1991).

[25] I. Egry, G. Lohöfer, I. Seyhan, S. Schneider, and B. Feuerbacher, "Viscosity and surface tension measurements in microgravity," Int. J. Thermophys. **20**, 1005–1015 (1999).

[26] I. Egry, A. Diefenbach, W. Dreier, and J. Piller, "Containerless processing in space—Thermophysical property measurements using electromagnetic levitation," Int. J. Thermophys. **22**, 569–578 (2001).

[27] W. Hembree, "High temperature rheology of Zr-based bulk metallic glass forming liquids," Ph.D. dissertation (Saarland University, 2015).

[28] I. Egry, H. Giffard, and S. Schneider, "The oscillating drop technique revisited," Meas. Sci. Technol. **16**, 426–431 (2005).

[29] G. Lohöfer, "Theory of an electromagnetically levitated metal sphere I: Absorbed power," SIAM J. Appl. Math. **49**, 567–581 (1989).

[30] C. A. Angell, "Formation of glasses from liquids and biopolymers," Science **267**, 1924–1935 (1995).

[31] R. Busch, E. Bakke, and W. Johnson, "Viscosity of the supercooled liquid and relaxation at the glass transition of the $Zr_{46.75}Ti_{8.25}Cu_{7.5}Ni_{10}Be_{27.5}$ bulk metallic glass forming alloy," Acta Mater. **46**, 4725–4732 (1998).

[32] J. C. Mauro, Y. Yue, A. J. Ellison, P. K. Gupta, and D. C. Allan, "Viscosity of glass-forming liquids," Proc. Natl. Acad. Sci. U. S. A. **106**, 19780 (2009).

[33] J. Wilden, F. Yang, D. Holland-Moritz, S. Szabó, W. Lohstroh, B. Bochtler, R. Busch, and A. Meyer, "Impact of sulfur on the melt dynamics of glass forming $Ti_{75}Ni_{25-x}S_x$," Appl. Phys. Lett. **117**, 013702 (2020).

[34] K. J. Laws, D. B. Miracle, and M. Ferry, "A predictive structural model for bulk metallic glasses," Nat. Commun. **6**, 8123 (2015).

[35] A. Inoue, "Stabilization of supercooled liquid and opening-up of bulk glassy alloys," Proc. Jpn. Acad., Ser. B **73**, 19–24 (1997).

[36] B. Bochtler, O. Gross, and R. Busch, "Indications for a fragile-to-strong transition in the high- and low-temperature viscosity of the $Fe_{43}Cr_{16}Mo_{16}C_{15}B_{10}$ bulk metallic glass-forming alloy," Appl. Phys. Lett. **111**, 261902 (2017).

[37] B. Bochtler, O. Gross, I. Gallino, and R. Busch, "Thermo-physical characterization of the $Fe_{67}Mo_6Ni_{3.5}Cr_{3.5}P_{12}C_{5.5}B_{2.5}$ bulk metallic glass forming alloy," Acta Mater. **118**, 129–139 (2016).

[38] S. Wei, M. Stolpe, O. Gross, W. Hembree, S. Hechler, J. Bednarcik, R. Busch, and P. Lucas, "Structural evolution on medium-range-order during the fragile-strong transition in $Ge_{15}Te_{85}$," Acta Mater. **129**, 259–267 (2017).

[39] C. Zhang, L. Hu, Y. Yue, and J. C. Mauro, "Fragile-to-strong transition in metallic glass-forming liquids," J. Chem. Phys. **133**, 014508 (2010).

[40] C. Zhou, L. Hu, Q. Sun, H. Zheng, C. Zhang, and Y. Yue, "Structural evolution during fragile-to-strong transition in CuZr(Al) glass-forming liquids," J. Chem. Phys. **142**, 064508 (2015).

[41] T. Hecksher, A. I. Nielsen, N. B. Olsen, and J. C. Dyre, "Little evidence for dynamic divergences in ultraviscous molecular liquids," Nat. Phys. **4**, 737–741 (2008).

[42] E. S. Park, J. H. Na, and D. H. Kim, "Correlation between fragility and glass-forming ability/plasticity in metallic glass-forming alloys," Appl. Phys. Lett. **91**, 031907 (2007).

[43] B. J. Keene, K. C. Mills, J. W. Bryant, and E. D. Hondros, "Effects of interaction between surface active elements on the surface tension of iron," Can. Metall. Q. **21**, 393–403 (1982).

04 April 2024 09:32:00